Preprint Title	Nano-scale friction and wear of polymer coated with graphene
Authors	Robin S. Vacher and Astrid S. de Wijn
Publication Date	29 Sep 2021
Article Type	Full Research Paper
ORCID® iDs	Robin S. Vacher - https://orcid.org/0000-0002-8048-3975; Astrid S. de Wijn - https://orcid.org/0000-0003-4664-6811

Nano-scale friction and wear of polymer coated with graphene

Robin Vacher*[1] and Astrid S. de Wijn[2]

Address: [1]Corrosion and tribology, SINTEF, Richard Birkelands vei 2B, 7034 Trondheim and [2]Institutt for maskinteknikk og produksjon, NTNU, Richard Birkelands vei 2B, 7034 Trondheim

Email: Robin Vacher - robin.vacher@sintef.no

* Corresponding author

Abstract

Background: Friction and wear of polymers at the nano scale is a challenging problem due to the complex viscoelastic properties and structure. Using molecular-dynamics simulations, we investigate how a graphene sheet on top of a semicrystalline polymer (PVA) affects the friction and wear.

Results: Our setup is meant to resemble an AFM experiment with a silicon tip. We have used two different graphene sheets: an unstrained, flat sheet, and one that has been crumpled before being deposited on the polymer.

Conclusion: The graphene protects the top layer of the polymer from wear and reduces the friction. The unstrained flat graphene is stiffer, and we find that it constrains the polymer chains and reduces the indentation depth.

Keywords

polymer; friction; graphene; molecular dynamics

Introduction

Graphene is a two dimensional material that has remarkable properties, both electronic [1,2] and mechanical [3,4]. Even before anything was known about graphene, the mechanical properties were already being utilised in engineering applications. Graphite powder, essentially thick flakes

of graphene, has been used as a lubricant additive for over a century to reduce wear and friction during sliding [5-7]. Nevertheless, we still don't understand all the different mechanisms at play in such systems. During the last few decades, with the development of the Atomic Force Microscope [8] and increases in computing power, it has become possible to investigate more deeply and develop understanding of the mechanisms that play a role in the friction of graphene (see, for example [9-21]). The effect of graphene coatings, and their ability to protect against wear, depends on the substrate underneath. Nevertheless, so far, they have been studied almost exclusively on metals [22,23]. Polymers coated with graphene have barely been studied on the nanoscale, due to the added complexity of the polymer, the tribology of which even without any coatings is still not well-understood [24,25]. In experiments, the tribology of polymer composite materials containing graphene has been studied with the goal of constructing a self-lubricating material [26]. Saravanan et al. [27] have measured the friction and wear of polymer materials such as PE (polyethylene), PC (polycarbonate), POM (polyoxymethylene), PMMA (polymethyl methacrylate), PEEK (polyetheretherketone) and PTFE (Polytetrafluoroethylene [28]). The polymers balls have been rubbed on a steel surface covered with layers of graphene oxide and PEI (polyethylenimine). They show that a transfer film of graphene on the polymer leads to lower friction. While to our knowledge there have been no numerical studies of friction on graphene coated polymers, the graphene polymer interface has been studied. Rissanou et al. [29,30] show that graphene has a strong effect on the structure and dynamics of the polymer chains near the interface. In this work, we aim to develop our understanding of the frictional behaviour of polymer coated with graphene by using molecular dynamics simulations of a single sliding asperity at the nanoscale. We show that graphene protects the polymer substrate from wear and identify the mechanism of this protection. We show that crumpling of the graphene has an impact on the friction. In section we first describe the simulation setup. Then we move on to discussing our simulations of depositing, indenting, and sliding on the graphene in section . Finally, we draw some conclusions in section .

Simulation setup

We simulate a slab of polyvinyl alcohol (PVA) coated with a single layer of graphene and a counterbody representing an AFM tip consisting of silicon. The simulations were peformed using LAMMPS [31]. We use the same setup for the polymer as our previous work [25], which we summarise below.

Interaction potentials

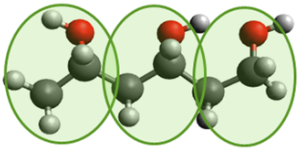

Figure 1: Coarse grained model for polyvenyl alcohol (PVA), $C_2H_4O)_x$. Red atoms are oxygens, dark gray are carbon, and clear gray are hydrogen. One green circle represents one coarse grained particle which replaces the group of atoms C_2H_4O

The PVA is described using a united-atom force field developed by Müller-Plathe et al. [32]. Each polymer particle represents a monomer of one structural unit (C_2H_4O) (see Fig. 1). The nonbonded interaction is given by a Lennard-Jones 96 potential $V_{\text{pair}}(r) = 4\epsilon_0[(\frac{\sigma_0}{r})^9 - (\frac{\sigma_0}{r})^6]$ where $\epsilon_0 = 0.0179$ eV, $\sigma_0 = 4.628$ Å, and r is the distance between the interacting monomers. The bonded interactions are described by a harmonic potential $V_{\text{bond}} = K(r - r_0)^2$ where $K = 2.37$ eV/Å^2 is the stiffness and $r_0 = 2.6$ Å is the equilibrium bond length. The bending potential is approximated by an angular potential described in a table format.

For graphene, we use the potential developed by O'Connor et al [33] (AIREBO-M potential). It is an empirical many-body potential that is directly implemented in LAMMPS.

$$V = \sum_i \sum_{j \neq i} E_{ij}^{\text{REBO}} + E_{ij}^{\text{LJ}} + \sum_{k \neq i,j} \sum_{l \neq i,j,k} E_{kijl}^{\text{TORSION}} \tag{1}$$

The interaction between the PVA and graphene is modelled using a Lennard-Jones 12-6 potential and Lorentz-Berlot mixing rule. $\sigma_1 = (\sigma_i + \sigma_j)/2 = 4.025$ Å, $\epsilon_1 = \sqrt{\epsilon_i \epsilon_j} = 0.015066$ eV.

a Flat graphene.

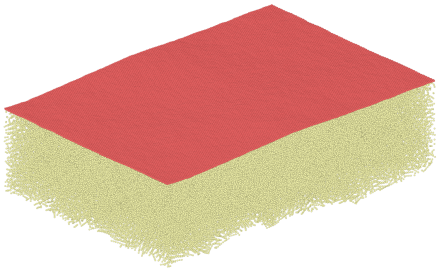

b Crumpled graphene.

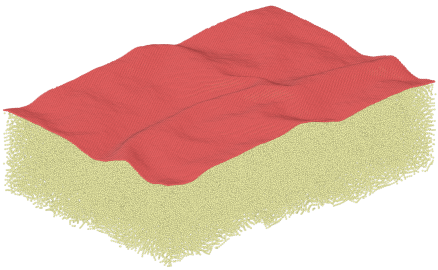

Figure 2: Snapshot of the simulation after the deposition of the graphene on the polymer and before indentation and sliding for **a**) the flat graphene and **b**) the crumpled graphene.

We model the interaction between the silicon tip and graphene using a Lennard-Jones 12-6 with the same parameters used by Li et al.[34]. $V_{\text{pair}}(r) = 4\epsilon_2[(\frac{\sigma_2}{r})^{12} - (\frac{\sigma_2}{r})^6]$ where $\epsilon = 0.092$ eV is the depth potential, and $\sigma_2 = 3$ Å is the distance at which the potential is equal to zero.

In our system, the tip and polymer are never in direct contact. They are always separated by graphene. We therefore do not need to model their interactions, but to be sure that no extremely unphysical events can occur, we have used the same potential as for the polymer-polymer interaction.

The masses of the particles were chosen to be equal to 12.01 g/mol for the carbon atom of graphene, 44.17 g/mol for the monomers in the PVA and, 2.8 g/mol for the particles of the FFM tip. This leads to a fairly small total tip mass. While this is not entirely physical, such a low mass will help speed up the dynamics and damping of the tip and save computation time without compromising the results[34]. We simulate the system with a time step of 1 fs.

Substrate cooling and characterization

We start from a box with periodic boundary conditions in the x and y direction (sizes 428 Å and 285 Å), filled up with PVA molecules placed randomly and constrained by hard walls in the z direction. The average density inside the polymer bulk is around 22 monomers/nm^3. The chains have a length of 50 monomers. Because there are overlaps, we initially give them no interaction. To remove overlapping gently, we first applied a nonphysical soft hybrid interaction potential, for 0.25 ns

to remove particle overlapping, and then slowly ramp up the potential over a period of 0.25 ns to the coarse-grained potential described in the previous section. The hybrid interaction potential consists of a 12–6 Lennard–Jones potential for the non-bonded interactions and a spring potential for the bonded interactions.

Once we have reached a melt with the correct interaction, we equilibrate it for 0.25 ns in the NVE ensemble. The temperature of the melt at this point is extremely high. To obtain a realistic semi-crystallized substrate structure, we cool down the sample using a Nosé-Hoover thermostat with a linearly decreasing temperature, starting at 5000 K down to 220 K with a cooling rate of 75 K/ns. After this, the temperature is kept constant at 220 K for 4 ns. At this point, we remove the walls and the z direction as they are no longer needed.

Graphene deposition

After the solidification of the semi-crystalline substrate, a layer of graphene is deposited on top. We use two different graphene sheets in our simulations. The first one is a single flat sheet of graphene that has the size of the box (Fig. 2a). The second one is also a single sheet, but the graphene has been crumpled by being compressed along x and y directions by 10%, which leads to wrinkles on the surface (Fig. 2b).

In both cases, we deposited the graphene on the surface of the polymer substrate by placing the graphene at around 90 Å from the surface and then applying a force to each of the graphene atoms equal to 0.00005 eV/Å (8.0×10^{-14} N) for a period of 75 ps, after which it sits on the surface and has stopped moving. The total normal force applied is around 4 nN (3.3 MPa). Then the force is removed and the graphene stays on the surface due to the adhesion.

Indentation and sliding procedure

In order to avoid sliding of the entire graphene sheet over the polymer substrate, we fix the position of some of the graphene atoms during the indentation and the sliding process. The two regions

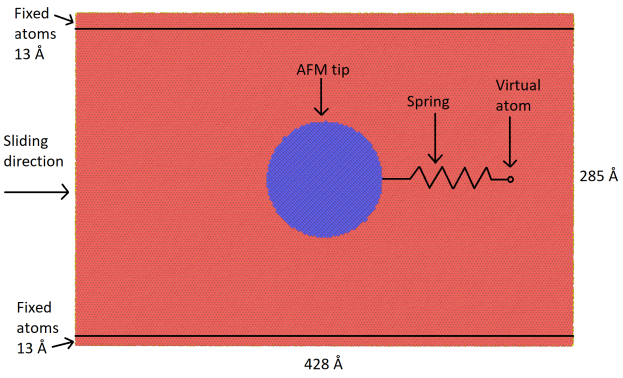

Figure 3: Top view of the simulation. The positions of the fixed graphene atoms are shown. The AFM tip is fixed to a support (virtual atom) via a spring, This support is moving at a constant speed in the sliding direction.

where the graphene atoms are fixed are located in strips along the x direction, which is the sliding direction, as far away as possible from the trajectory of the tip (Fig. 3).

The FFM tip is rigid and consists of atoms arranged in an fcc lattice with a period of 5.43 Å, which is the crystal structure of silicon. A semisphere is cut out from this material. The tip is placed above the surface. A constant normal force is applied to the tip so that it moves towards and indents the surface. After 1 ns, the tip has reached a stable depth. The tip is then attached to the support with a harmonic spring along the sliding direction. The spring constant is equal to 30 N/m. The support is moving at a constant horizontal velocity of 2 m/s. We run the sliding simulation for a distance of 100 Å, which takes roughly 6000 CPUcore hours.

Method of analysis

The box is divided into a grid that moves with the tip. During sliding, we bin the individual polymer particles depending on their position in the reference frame of the tip. This enables us to create heat maps of average properties around the tip, such as the density or the average displacements of the particles.

We calculate the surface roughness of the top polymer atoms. We first divide the box into bins of size σ_0 in both x and y. Each bin is assigned the height of the atom with the highest z position. We

finally compute the surface roughness as the root mean square height of a given area,

$$S_q = \sqrt{\frac{1}{A}\sum\sum Z^2(x,y)\Delta x \Delta y}\,, \tag{2}$$

where A is the surface area and Z is the height of the particles on the surface.

Results and Discussion

Graphene deposition

After the deposition of graphene, we investigate its effect on the surface. The deposited graphene alters the structure and shape of the surface. This can be seen in Fig. 4, where we show the density as a function of the position in a cross-section of the substrate for the cases with and without a graphene layer.

We characterise the shape of the polymer surface by the roughness. We computed the roughness of the bare surface, as well as surfaces covered in flat and crumpled graphene just after the deposition. Before the deposition of graphene, the roughness of the polymer surface is equal to 0.543 Å. After the deposition of the flat graphene, the roughness decreases to 0.186 Å. After deposition of the crumpled graphene, the roughness changes to 0.581 Å. The flat graphene flattens the surface, while the crumpled graphene accommodates to it.

In addition to the shape, the structure of the polymer near the surface is affected by the graphene. In the case of the flat graphene, the particles of the polymer align in layers parallel to the surface, as can be seen in Fig. 4b. In Figure b), the red flat region corresponds to a depth at which there is a high density of polymers. A similar effect has been observed for other polymers as well [29,30]. For the crumpled graphene, the structure of the polymer is not as strongly affected by the deposition (Fig. 4c), though there is some sign of it.

Indentation

After the graphene is deposited, we add the AFM tip to our simulation and indent it into the surface. Figure 5 shows the indentation depth as a function of time for a normal load of 6.4 nN on the flat graphene. Different loads have been applied in the range 1-100 nN. The depth was determined as the distance between the lowest atom of the tip and the average height of the graphene sheet before indentation minus the tip-graphene interaction equilibrium distance σ_2. We have performed this type of analysis for two different radii, 50 and 100 Å. The sliding starts directly after the indentation process.

We have run a long indentation simulation with a load of 6.4nN to determine the penetration depth after a long period of time (see Fig. 5). We only observe a slight increase in the depth between 1 ns and 4 ns of around 1 Å. Thus, we consider the tip indented fully after 1ns.

The indentation depth depends strongly on the load, as expected (Fig. 6). At low normal force, the tip with a higher radius penetrates deeper due to adhesion, which contributes significantly to the effective load force by pulling the tip into the surface. At higher loads, the smaller tip penetrates further, as it is subjected to larger external pressure. In the case of the crumpled graphene, we see a larger indentation depth compare to the flat graphene (Fig. 8). The tip has more freedom to sink inside the material when the graphene is crumpled (membrane buckling) than in a case of flat graphene (stiff membrane).

Figure 7 shows the cross-section of the density under the tip at the end of the indentation process. We can see regular lines of high density right below the graphene which indicate a local reorganisation of the polymer chains. The graphene, especially the flat sheet, is also curved away from the tip a little, which plays a role in reducing the local pressure comparing to the case with no graphene.

Frictional forces

Once the tip is sufficiently indented into the surface (after 1 ns), we start the sliding. Figure 10 shows the lateral force as a function of the displacement of the support in the case of the flat graphene.

To better highlight the influence of the tip radius, we average the frictional forces between the support displacement 50 and 100 Å. We plot those results as a function of the normal load for two different tip sizes (radius of 50 and 100 Å) in Fig. 11. We observe a regular stick-slip motion. The distance between sticks corresponds to one lattice period of the graphene.

We observe in Fig. 10 that for the highest loads the frictional force increases during sliding. This may be due to local frictional heating leading to a change in mechanical properties of the polymer below the tip.

In the case of the crumpled graphene (Fig. 12), the frictional curve is subject to more fluctuations. The calculation of the average frictional force taken between support displacements 50 and 100 Å (Fig. 14) shows the strong impact of the flexibility of the graphene. Again, the higher indentation depth of the tip leads to a stronger frictional force (2 to 3.5 times).

We compare this to sliding without graphene. In a simulation with no graphene, a normal load of 51 nN, and a tip radius of 100 Å, we found that the tip moves deeply inside the substrate and the average friction is above 90nN, almost an order of magnitude higher than with graphene. This clearly shows that the graphene layer darstically reduces the friction.

To observe the effect of sliding on the wear of the polymer material, we compare three simulations: one without graphene, one with flat graphene, and one with crumpled graphene. All have a normal load of 1 nN and a tip radius of 50 Å (Fig. 13). To improve the averaging by increasing the total sliding distance, we increase the sliding speed by a factor 10 to 20 m/s. The displacement vectors are recorded after 0.6 ns, meaning that the support has moved 120 Å. This is indicated by the dashed and solid lines. Without graphene, the vector displacements close to the surface are high and in the sliding direction, this indicates that strong residual deformation remains at the surface because of the shearing of the chains. We observe that the displacements of the polymer are

roughly an order of magnitude less when graphene is present. This indicates that graphene efficiently prevents damage of the substrate. The displacements are the smallest in the case of the flat graphene sample, where the graphene is not just protecting the polymer from the tip, but also constraining the chains.

The graphene we have used, both flat and crumpled, is constrained to remain at a specific length because of the periodic boundary conditions of the simulation box. This means that any elastic stretching of the graphene sheet is limited to a fairly small area. In reality, most of the graphene sheets are larger than the length of our simulation box and depending on how they attach to the surface, they may thus have more length to stretch elastically. Our crumpled graphene, by having a longer equilibrium length than the box, is more representative of completely unconstrained, loose, graphene sheets. However, graphene that is bound to the polymer surface, through adhesion or covalent chemical bonds, would behave more like the flat graphene in our simulations, and provide additional protection.

Conclusion

We simulate friction force microscope experiments with molecular dynamics. A rigid counterbody simulating the tip of the FFM is rubbed against a substrate made of a semicrystalline polymer (PVA) with a graphene sheet on top. Doing such simulations enables us to understand some of the mechanisms at play in such systems. Two different graphene sheets have been investigated: a flat graphene that has the same size as the simulation box and a crumpled graphene sheet that has been bi-axially compressed by 10%. Before and after the sheet is deposited on the substrate, we computed the roughness. We can observe that the crumpled graphene accommodates to the roughness of the polymer, while the flat graphene reduces the roughness. We also observe a rearrangement of the chain near the surface into a layered structure, indicating that the chains tend to align parallel to the surface. During sliding, the tip sink slowly into the material. This sinking affects the real surface area and has a noticeable effect on the friction when the normal load is high. The displacements of the chains are roughly an order of magnitude less when a graphene sheet is present com-

pared to the case with no graphene. Since this is where the most severe wear occurs the graphene therefore reduces wear. We can see that the graphene is curved away from the tip, this is especially true for the flat graphene. This helps to spread out the pressure, and reduce the local pressure in the polymer. The flat graphene is the most efficient at reducing the friction and wear of the system by this mechanism, as it is harder to penetrate.

Acknowledgements

We acknowledge IDUN cluster at NTNU and Sigma2 (project NN9573K) for providing the computational power. This work was funded by the Research Council Norway (NFR) grant Number 259869. We are grateful to Sergio Armada for his support and discussions.

a Density before deposition of the graphene sheet.

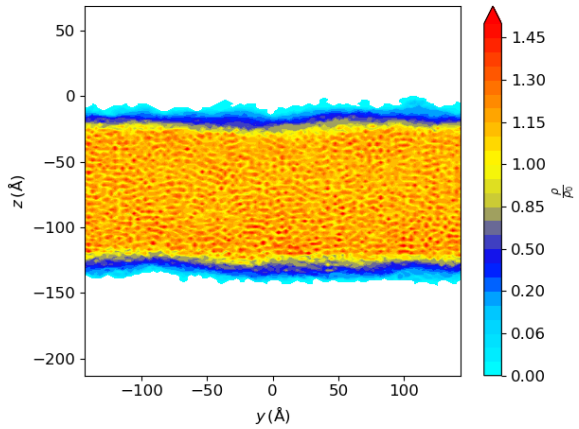

b Density after deposition of the flat graphene sheet.

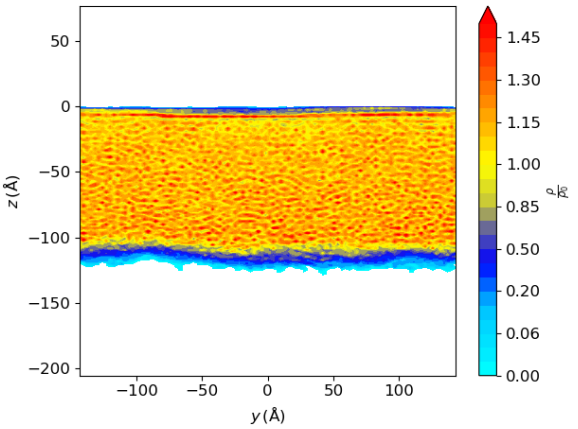

c Density after deposition of the crumpled graphene sheet.

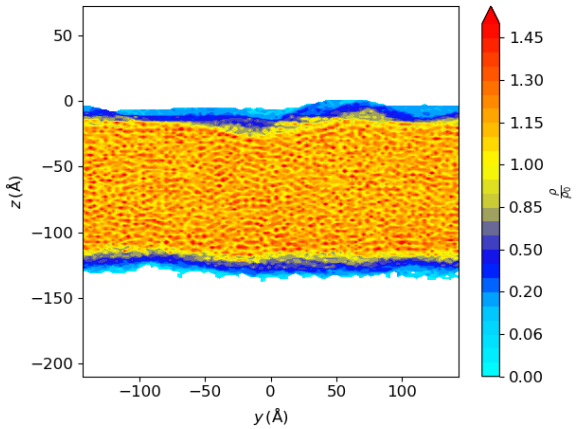

Figure 4: Density of the substrate through the full length of the simulation box (polymer only), **a**) before deposition of the graphene, **b**) after deposition of the flat graphene, and **c**) after deposition of the crumpled graphene. The graphene affects the roughness and structure of the substrate.

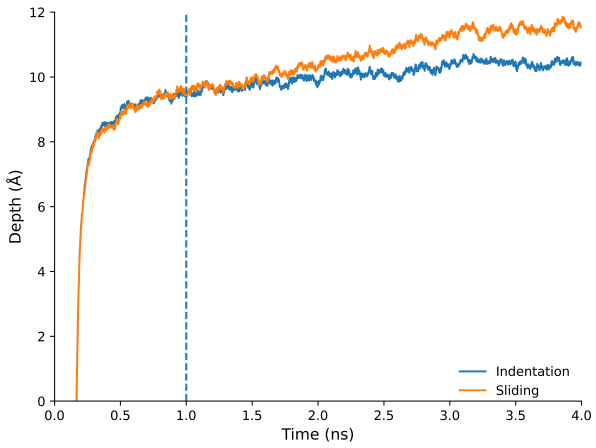

Figure 5: The penetration depth versus time for a long indentation and for the sliding process, for a tip with radius 50 Å and load 6.4 nN (4 eV/Å), on the flat graphene. The dashed line represents the time at which we measure the indentation depth and compare this value with other simulations. The sliding process is starting after the dashed line. Without sliding the tip does not indent much further, but with sliding it does.

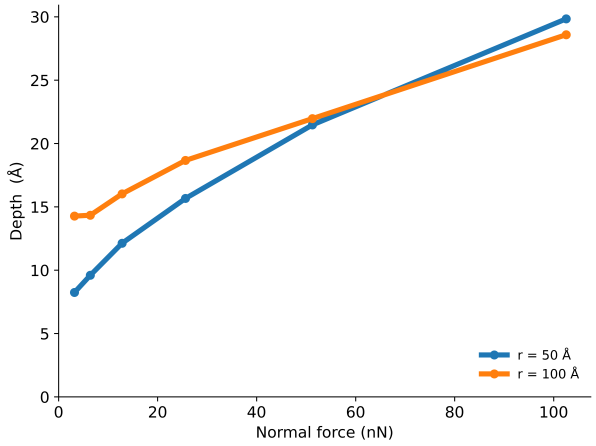

Figure 6: Indentation depth as a function of the normal load for the flat graphene specimen with a tip radius r = 50 Å and 100 Å.

a Density of the polymer for the flat graphene, r=50 Å, F_n=3.2 nN.

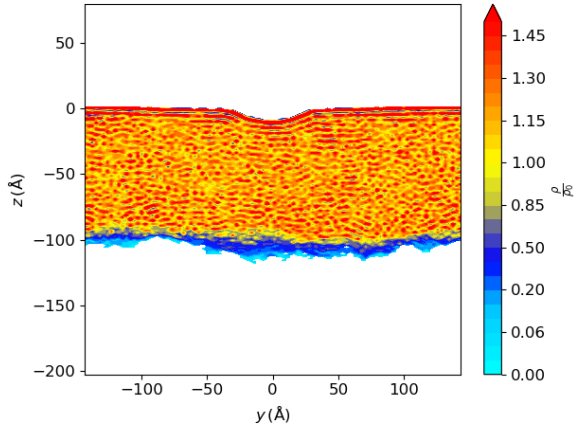

b Density of the polymer for the flat graphene, r=100 Å, F_n=12.8 nN.

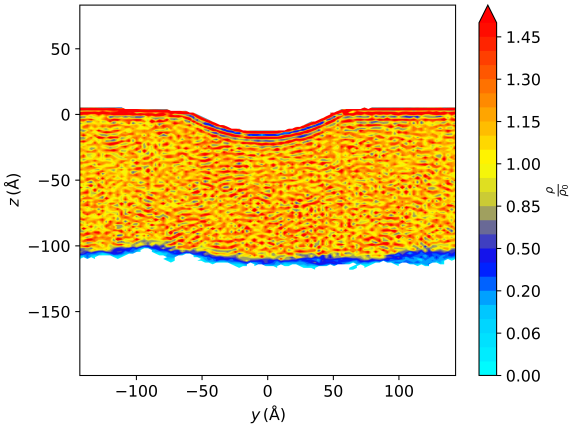

c Density of the polymer for the crumpled graphene, r=50 Å, F_n=3.2 nN.

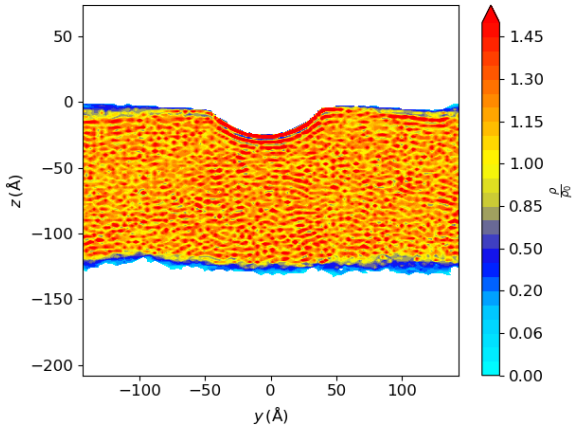

Figure 7: Density maps of the polymer for **a**) the flat graphene with r=50 Å and F_n=3.2 nN, **b**) the flat graphene with r=100 Å and F_n=12.8 nN, and **c**) the crumpled graphene with r=50 Å and F_n=3.2 nN. The cuts are taken right bellow the middle of the tip on a small thickness (14 Å). The tip indents further on the crumpled graphene.

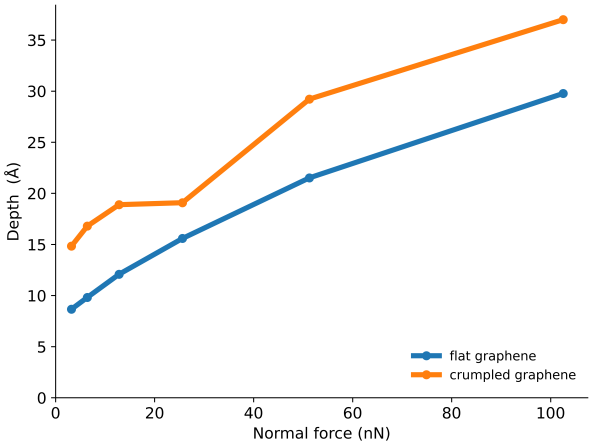

Figure 8: Indentation depth of the flat graphene and crumpled graphene for different normal loads and a tip radius of r = 50 Å.

a Flat graphene sheet.

b Crumpled graphene sheet.

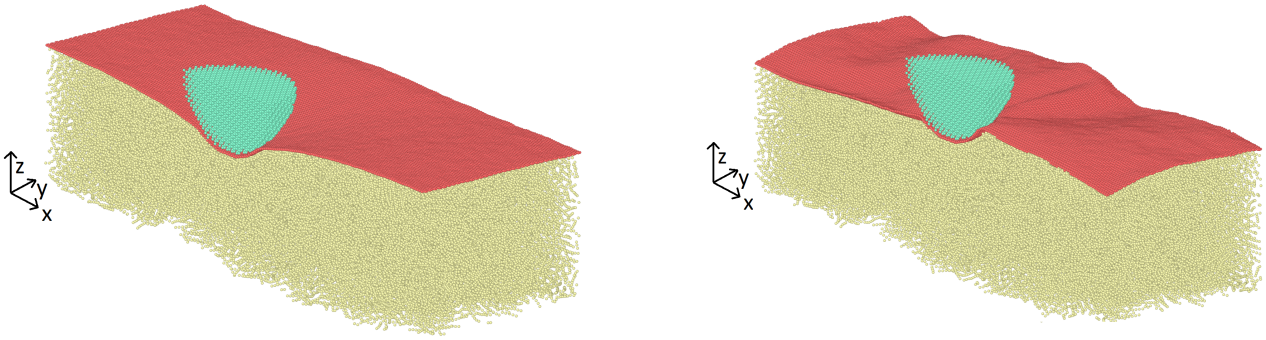

Figure 9: Snapshots of the simulation during sliding for a tip radius of 50 Å and a load of 102 nN (64 eV/Å) for **a**) the flat graphene, and **b**) the crumpled graphene.

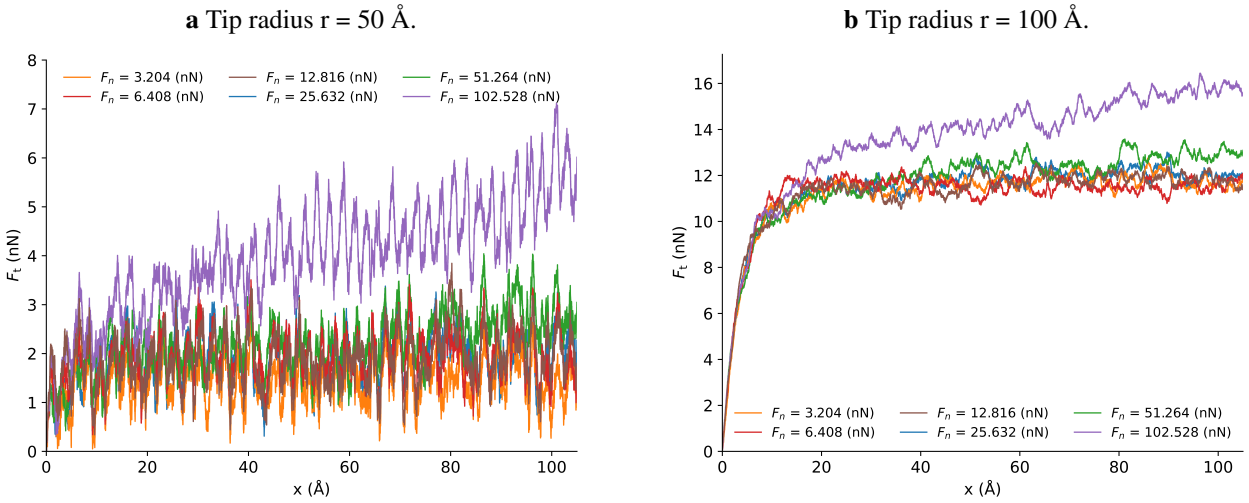

Figure 10: Frictional force versus the position of the support on the flat graphene specimen for **a**) a tip radius r = 50 Å, and **b**) a tip radius r = 100 Å.

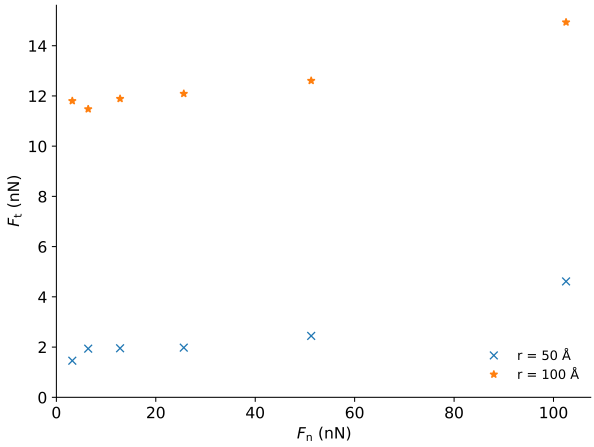

Figure 11: Average frictional force measured between support displacement 50 and 100 Å of the support displacement versus load applied for a tip radius of 50 and 100 Å on the flat graphene specimen. For comparison, in a simulation with no graphene, a normal load of 51 nN, and a tip radius of 100 Å, we find an average friction above 90nN.

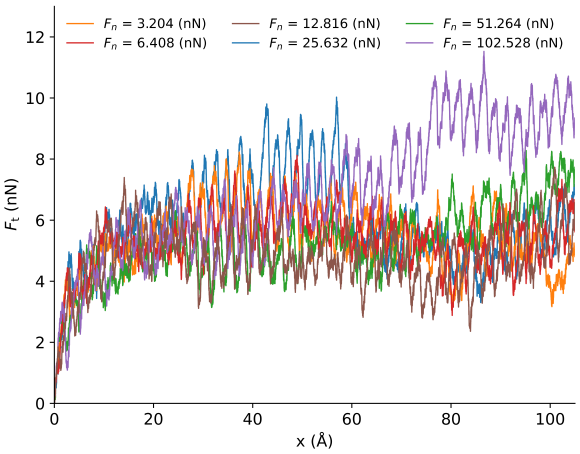

Figure 12: Frictional force versus the position of the support for a tip of radius r = 50 Å, on the crumpled graphene specimen.

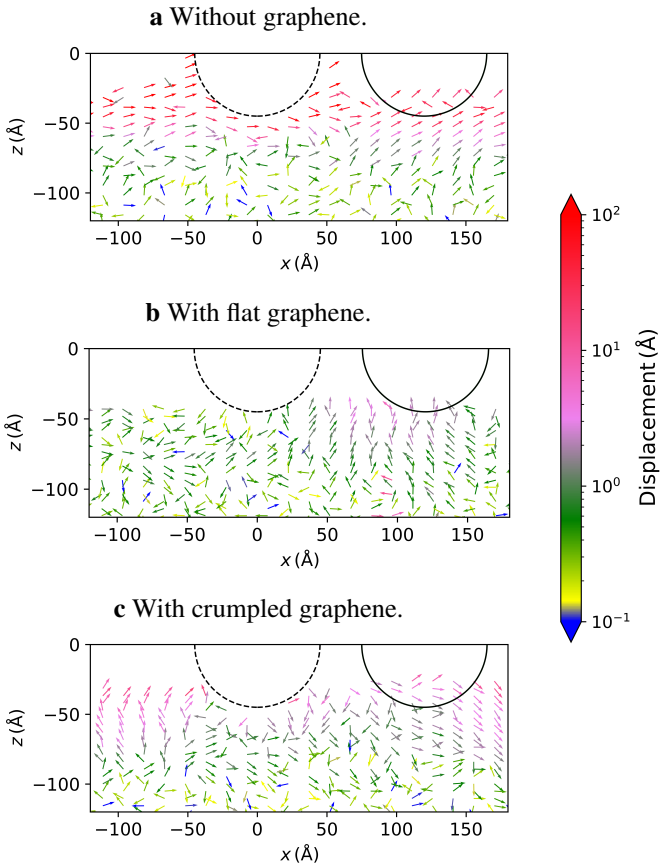

Figure 13: Average displacement of the atoms bellow the tip during sliding for **a** the case without graphene, **b** the flat graphene, and **c** the crumpled graphene.

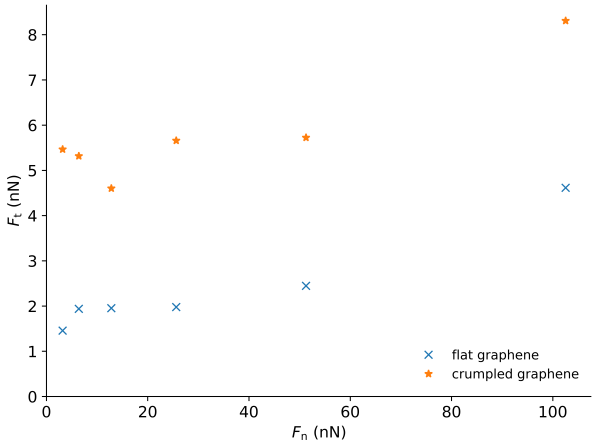

Figure 14: Average frictional force measured between 50 and 100 Å of the support displacement versus load applied for a tip radius r=50 Å on the crumpled and flat graphene.

References

1. Saxena, S.; Tyson, T. A.; Shukla, S.; Negusse, E.; Chen, H.; Bai, J. *Applied Physics Letters* **2011**, *99* (1), 013104.

2. Ando, T. *NPG asia materials* **2009**, *1* (1), 17–21.

3. Berman, D.; Erdemir, A.; Sumant, A. V. *Materials Today* **2014**, *17* (1), 31–42. doi:https://doi.org/10.1016/j.mattod.2013.12.003.

4. Lee, C.; Wei, X.; Li, Q.; Carpick, R.; Kysar, J. W.; Hone, J. *physica status solidi (b)* **2009**, *246* (11-12), 2562–2567.

5. Penkov, O.; Kim, H.-J.; Kim, H.-J.; Kim, D.-E. *International journal of precision engineering and manufacturing* **2014**, *15* (3), 577–585.

6. Lee, H.; Lee, N.; Seo, Y.; Eom, J.; Lee, S. *Nanotechnology* **2009**, *20* (32), 325701.

7. Peng, Y.; Wang, Z. *RSC Advances* **2014**, *4* (20), 9980–9985.

8. Binnig, G.; Quate, C. F.; Gerber, C. *Phys. Rev. Lett.* **1986**, *56*, 930–933. doi:10.1103/PhysRevLett.56.930.

9. Filleter, T.; McChesney, J. L.; Bostwick, A.; Rotenberg, E.; Emtsev, K. V.; Seyller, T.; Horn, K.; Bennewitz, R. *Phys. Rev. Lett.* **2009**, *102*, 086102. doi:10.1103/PhysRevLett.102.086102.

10. Li, J.; Cao, W.; Li, J.; Ma, M.; Luo, J. *The Journal of Physical Chemistry Letters* **2019**, *10* (11), 2978–2984. doi:10.1021/acs.jpclett.9b00952. PMID: 31094522

11. Kawai, S.; Benassi, A.; Gnecco, E.; Söde, H.; Pawlak, R.; Feng, X.; Müllen, K.; Passerone, D.; Pignedoli, C. A.; Ruffieux, P.; Fasel, R.; Meyer, E. *Science* **2016**, *351* (6276), 957–961. doi:10.1126/science.aad3569.

12. Wang, L.; Zhou, X.; Ma, T.; Liu, D.; Gao, L.; Li, X.; Zhang, J.; Hu, Y.; Wang, H.; Dai, Y.; Luo, J. *Nanoscale* **2017**, *9*, 10846–10853. doi:10.1039/C7NR01451A.

13. van Wijk, M. M.; Dienwiebel, M.; Frenken, J. W. M.; Fasolino, A. *Phys. Rev. B* **2013**, *88*, 235423. doi:10.1103/PhysRevB.88.235423.

14. Chandross, M.; Lorenz, C. D.; Stevens, M. J.; Grest, G. S. *Langmuir* **2008**, *24* (4), 1240–1246. doi:10.1021/la702323y. PMID: 18184018

15. Dienwiebel, M.; Verhoeven, G. S.; Pradeep, N.; Frenken, J. W. M.; Heimberg, J. A.; Zandbergen, H. W. *Phys. Rev. Lett.* **2004**, *92*, 126101. doi:10.1103/PhysRevLett.92.126101.

16. Van Wijk, M.; Dienwiebel, M.; Frenken, J.; Fasolino, A. *Physical review. B, Condensed matter* **2013**, *88*, 235423. doi:10.1103/PhysRevB.88.235423.

17. Kawai, S.; Benassi, A.; Gnecco, E.; Söde, H.; Pawlak, R.; Feng, X.; Müllen, K.; Passerone, D.; Pignedoli, C. A.; Ruffieux, P. et al. *Science* **2016**, *351* (6276), 957–961.

18. Penkov, O.; Kim, H.-J.; Kim, H.-J.; Kim, D.-E. *Int. J. Precis. Eng. Manuf.* **2014**, *15*, 577–585. doi:10.1007/s12541-014-0373-2.

19. Li, Q.; Lee, C.; Carpick, R. W.; Hone, J. *physica status solidi (b)* **2010**, *247* (11-12), 2909–2914.

20. Lee, C.; Li, Q.; Kalb, W.; Liu, X.-Z.; Berger, H.; Carpick, R. W.; Hone, J. *science* **2010**, *328* (5974), 76–80.

21. Andersson, D.; de Wijn, A. S. *Nature communications* **2020**, *11* (1), 1–7.

22. Liao, Y.; Pourzal, R.; Wimmer, M.; Jacobs, J.; Fischer, A.; Marks, L. *Science* **2011**, *334* (6063), 1687–1690.

23. Berman, D.; Erdemir, A.; Sumant, A. V. *Carbon* **2013**, *54*, 454–459. doi:https://doi.org/10.1016/j.carbon.2012.11.061.

24. Zeng, X.; Peng, Y.; Liu, L.; Lang, H.; Cao, X. *Nanoscale* **2018**, *10*, 1855–1864. doi:10.1039/C7NR07517K.

25. Vacher, R.; de Wijn, A. S. *Tribology Letters* **2021**, *69* (1), 1–12.

26. Huang, T.; Li, T.; Xin, Y.; Jin, B.; Chen, Z.; Su, C.; Chen, H.; Nutt, S. *RSC advances* **2014**, *4* (38), 19814–19823.

27. Saravanan, P.; Selyanchyn, R.; Tanaka, H.; Fujikawa, S.; Lyth, S. M.; Sugimura, J. *Carbon* **2017**, *122*, 395–403. doi:https://doi.org/10.1016/j.carbon.2017.06.090.

28. Kandanur, S.; Rafiee, M.; Yavari, F.; Schrameyer, M.; Yu, Z.-Z.; Blanchet, T.; Koratkar, N. *Carbon* **2012**, *50*, . doi:10.1016/j.carbon.2011.10.038.

29. Rissanou, A. N.; Harmandaris, V. *Soft Matter* **2014**, *10* (16), 2876–2888.

30. Rissanou, A.; Harmandaris, V. *Journal of Nanoparticle Research* **2013**, *15*, . doi:10.1007/s11051-013-1589-2.

31. *LAMMPS Stable release 29 October 2020*, stable_29Oct2020; Zenodo, 2020. doi:10.5281/zenodo.4157471.

32. Meyer, H.; Müller-Plathe, F. *Macromolecules* **2002**, *35* (4), 1241–1252. doi:10.1021/ma011309l.

33. O'Connor, T. C.; Andzelm, J.; Robbins, M. O. *The Journal of Chemical Physics* **2015**, *142* (2), 024903. doi:10.1063/1.4905549.

34. Li, S.; Li, Q.; Carpick, R. W.; Gumbsch, P.; Liu, X. Z.; Ding, X.; Sun, J.; Li, J. *Nature* **2016**, *539* (7630), 541–545.